ADVANCED MATERIALS TECHNOLOGIES
www.advmattechnol.de

Ultra-Sensitive Bio-Polymer Iontronic Sensors for Object Recognition from Tactile Feedback

*Melih Ogeday Cicek, Mete Batuhan Durukan, Bayram Yıldız, Deniz Keskin, Doga Doganay, Simge Çınar Aygün, Murat Perit Cakir, and Husnu Emrah Unalan**

Supramolecular polymer gels show promise for use in batteries, supercapacitors, and multifunctional sensors. However, their poor stiffness and ionic conductivity hinder their large-scale utilization. Herein, a cellulose-based supramolecular bio-polymer gel (SBPG) with high ionic conductivity and exceptional stiffness is reported. These properties are translated into proof-of-concept iontronic pressure sensors with an ultra-high sensitivity of 1 475 000 kPa^{-1}. The technological potential is demonstrated via fabrication of a prototype smart glove using only eight pressure sensors based on this novel gel. Smart glove sensors with 90% classification accuracy for object recognition are demonstrated using a tactile feedback algorithm.

1. Introduction

Rapidly developing robotics, human–machine interface devices, and wearable electronics necessitate mechanically flexible and highly sensitive pressure sensors with a compact, and user-friendly design.[1–7] Pressure sensors typically convert mechanical input from the environment into electrical signals based on triboelectric,[8] capacitive,[9] resistive,[10] and iontronic[11] principles. Iontronic pressure sensors have high sensitivity and fast response.[12] The formation of a polarization-dependent electrical double layer (EDL) on the surface of electrodes enables iontronic pressure sensors to achieve high capacitance change under applied pressure. Moreover, the high capacitance in the iontronic pressure sensors increases the resolution of the measured data by minimizing the parasitic effects from the environment. These aspects of iontronic sensors make them ≈10 000 times more sensitive than capacitive pressure sensors.[13,14]

Iontronic pressure sensors are expected to play a key role in virtual reality as a tactile feedback interface.[12] Their use have been demonstrated in amputee prosthesis,[15] sensing units for soft robots,[16] body motion monitoring[13] and wearable healthcare products.[17] Despite recent advances, the use of iontronic pressure sensors for object recognition from tactile feedback has remained elusive.[18,19] There are articles in the literature that can show pressure distributions in contact with objects using a small number of sensors with limited sensitivity. However, these articles generally focus on extracting pressure distributions generated by a small number of objects with completely different shapes.[11,20] Successful recognition of large numbers of objects can only be achieved using multiple sensor pairs and complex electronics due to the low sensitivity of the sensors.[21] This complexity negatively affects user comfort and complicates data collection/processing. Another problem with low-sensitivity is a limited capacitive operating range and a correspondingly low signal-to-noise ratio. Data from sensor pairs are very close to each other due to limited capacitance change, which limits the sensors' ability to recognize objects of similar shape. Moreover, the parasitic effect is a critical problem for low-sensitivity capacitive sensors operating with pF-level capacitance. This parasitic effect may be due to environmental conditions such as temperature and humidity, as well as the connections of the sensors, the cables used for data transfer, and other sensor pairs used for object recognition. In addition to all these, the material of the object in contact can also have a parasitic effect. Thus, it is important to develop for iontronic pressure sensors with enhanced sensitivity while maintaining structural flexibility.

We describe the use of a rationally designed supramolecular bio-polymer gel (SBPG) based on hydroxyethyl cellulose (HEC), glycerol, and NaCl (Figure S1, Supporting Information) as the dielectric layer for touch-mode iontronic pressure sensors. The self-assembly of HEC and glycerol molecules is optimized to obtain the highest possible ionic conductivity, areal capacitance with

M. O. Cicek, M. B. Durukan, B. Yıldız, D. Keskin, D. Doganay, S. Çınar Aygün, H. E. Unalan
Department of Metallurgical and Materials Engineering
Middle East Technical University (METU)
Ankara 06800, Turkey
E-mail: unalan@metu.edu.tr
M. B. Durukan, S. Çınar Aygün, H. E. Unalan
Energy Storage Materials and Devices Research Center (ENDAM)
Middle East Technical University (METU)
Ankara 06800, Turkey
M. P. Cakir
Department of Cognitive Science, Graduate School of Informatics
Middle East Technical University (METU)
Ankara 06800, Turkey
M. P. Cakir
Modelling & Simulation Research Center (MODSIMMER)
Middle East Technical University (METU)
Ankara 06800, Turkey
The ORCID identification number(s) for the author(s) of this article can be found under https://doi.org/10.1002/admt.202300322

DOI: 10.1002/admt.202300322

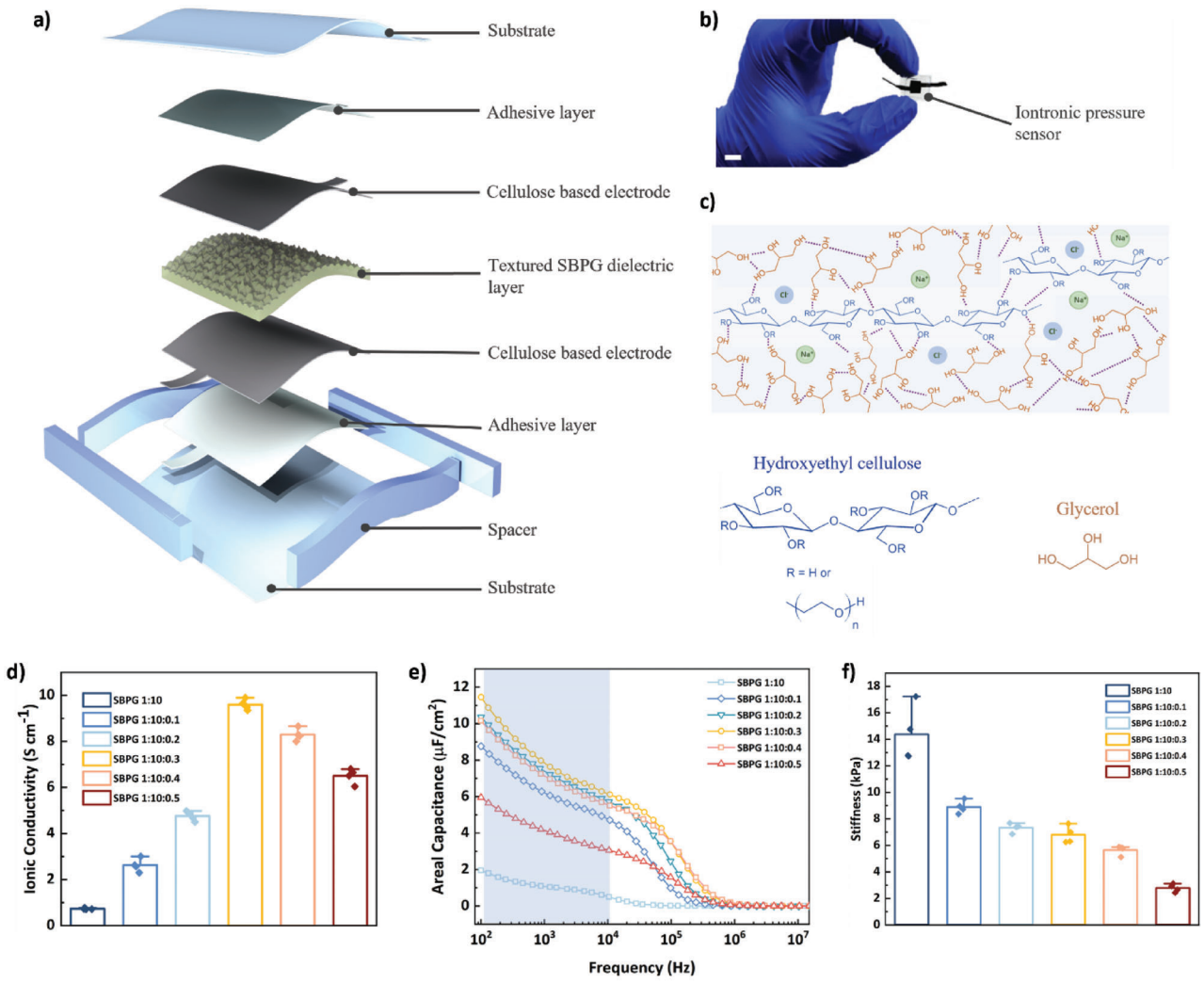

Figure 1. a) Hierarchical structure of the iontronic pressure sensor. b) Photograph of the fabricated sensor (Scale bar corresponds to 1 cm). c) Schematic diagram illustrating the supramolecular bio-polymer gel structure. Dashed lines indicate the hydrogen bonds that occur between HEC chains and the glycerol molecules. d) Ionic conductivity measurements of SBPGs with different NaCl contents. e) Areal capacitance measurements of the SBPGs with different NaCl contents between 100 Hz and 15 MHz. Shaded area shows the frequency range that EDL can still exists. Shaded area indicates the working frequency of our sensors. f) Stiffness values of the SBPGs with different NaCl contents.

sufficient stiffness from the SBPGs. The effects of the tunable electrochemical properties on the sensing performance and sensing mechanism of the iontronic pressure sensors are addressed. This fundamental breakthrough in the fabrication of the sensor's dielectric layer enables the creation of field-leading, ultrasensitive iontronic pressure sensors. Moreover, a prototype smart glove is fabricated using only eight sensing units. This smart glove is used to distinguish objects of similar shape but different sizes and weights with high accuracy, relying on tactile feedback obtained from pressure sensors.

2. Results and Discussion

2.1. Characterization of the SBPGs

The hierarchical structure of the fabricated iontronic pressure sensors includes four major components: substrate, spacer, carbon-based electrode layers, and textured SBPG (**Figure 1**a). A photograph of the sensor is provided in Figure 1b. Photographs of the textured dielectric and carbon-based electrode layers are provided in Figures S2a,b and S3 (Supporting Information). Fabricated SBPGs are used as dielectric layers for ultrasensitive iontronic pressure sensors. Detailed structural analyses through Fourier Transform Infrared Spectroscopy (FTIR) revealed that the supramolecular nature of the SBPG enables HEC and glycerol molecules to form dynamic hydrogen bonding (Figures S4–S6 and Text S1, Supporting Information). This allows ions to move freely through the structure (Figure 1c).

The intrinsic properties of the SBPGs are crucial to understand the high performance of pressure sensors. Therefore, we characterized ionic conductivity, areal capacitance, and the stiffness of the SBPGs in detail. Impedance spectroscopy is used to calculate ionic conductivity of the SBPGs, results of which are provided in Figure S7a,b (Supporting Information). The ionic conductivity of

the gels with different stoichiometries is calculated and provided in Figure 1d (also provided in Figure S8, Supporting Information). We first investigate the ionic conductivity of HEC-glycerol SBPGs and the highest ionic conductivity of 7.72×10^{-5} S cm^{-1} is obtained at a HEC:glycerol ratio of 1:10. The ionic conductivity is then gradually decreased with the glycerol content, as can be seen in Figure S8 (Supporting Information). Therefore, SBPG with a HEC:glycerol ratio of 1:10 is referred to as an "ideal" structure. The main reason for this is the formation of the glycerol islands in the structure when the glycerol content exceeds a certain value. TGA results of the SBPGs further clarified the observed behavior (Text S2 and Figure S9a, Supporting Information). An extra decomposition step begins to be observed in samples with glycerol ratios above the ideal structure. This extra step belongs to non-HEC-bound glycerol islands.

Next, the effect of ions on the conductivity is investigated over the ideal structure. NaCl is added as an ion source using the stoichiometric ratios provided in Table S1 (Supporting Information). With increased NaCl content, the ionic conductivity is gradually increased to 9.85×10^{-4} S cm^{-1} (for SBPG 1:10:0.3). Further increase in NaCl content adversely affected the ionic conductivity and decreased it to 6.92×10^{-4} S cm^{-1} (for SBPG 1:10:0.5) as shown in Figure 1d. The number of free ions determine the ionic conductivity. Therefore, it is reasonable to expect low conductivities from SBPGs with low NaCl content. However, an increase in the salt concentration has a detrimental effect on the ionic conductivity. X-Ray diffraction (XRD) analysis showed that SBPGs are in amorphous nature and the addition of NaCl do not change the structure (Figure S10a,b, Supporting Information). Therefore, the observed deterioration may be related to ion cluster formation due to increased ion density[22] and consumption of number of vacancies for ion transport.[23]

The areal capacitance depends on the number of free ions and the polar groups of the polymer chains. High areal capacitance is attributed to the charge accumulation at electrode–electrolyte interface up to the charge relaxation frequency as shown in Figure 1e, Figure S11, and Text S3 (Supporting Information). Above this frequency, free ions cannot orient themselves with the applied electric field, causing a sudden decrease in areal capacitance. Therefore, one has to confine the working frequency of the sensors. Shaded area in Figure 1e indicates the most efficient working frequency range of the iontronic pressure sensors. In this range, the main capacitive contribution comes from free ions and oriented dipoles, and high capacitance values can be achieved.

The high performance and stability of the sensor rely heavily on the mechanical properties of the SBPGs. Therefore, we conducted oscillatory rheometry analysis for SBPGs, results of which are provided in Figure S12 (Supporting Information) validating their gel-like behavior (Text S4, Supporting Information). The value of the storage modulus at the lowest applicable frequency corresponds approximately to stiffness value measured in a static test.[24,25] Stiffness values of the SBPGs are provided in Figure 1f and Figure S13 (Supporting Information). A gradual decrease in stiffness is observed with increasing NaCl content. This demonstrates the disruption of the intermolecular interactions between glycerol molecules and the HEC chains. The disruption is also confirmed by TGA results (Text S2 and Figure S9, Supporting Information). We have also compared the stiffness of the SBPGs with that of human tissues (Figure S14, Supporting Information). The stiffness range of SBPGs is wider than that of human skin, which indicates that the gels we produce can withstand the mechanical effects that the skin is exposed to. Therefore, SBPGs provide the necessary strength for a pressure sensor to be used in the recognition of common objects.

2.2. Characterization of Iontronic Pressure Sensor

The pressure sensor is working in touch mode capacitive sensing as developed by Ko and co-workers and well-studied in the literature.[26,27] In this architecture, upper electrode layer is separated from the dielectric layer of the structure. This architecture is also adapted for iontronic pressure sensors.[13,20] For the fabrication of state-of-art touch-mode wearable iontronic pressure sensors the benchmark values for ionic conductivity, areal capacitance and stiffness for the dielectric layers can be set at 2×10^{-4} S cm^{-1}, 5 μF cm^{-2}, and 10 kPa, respectively. In addition, they should consume low power to be used effectively in wearable devices. Devices should also show high mechanical stability with a sensitivity above 1 000 000 kPa^{-1}. Here we report SBPGs that meet or even exceed these parameters. This allowed us to fabricate iontronic pressure sensors with unprecedented sensitivity and stability (sensitivity of 1 475 000 kPa^{-1}). In addition, the peak operating power of the fabricated sensor was calculated as 4 μW (Text S5, Supporting Information).

Firstly, the sensitivity of iontronic pressure sensors is tested on a control group containing untextured SBPGs and carbon-based electrodes. The importance of the stiffness of the SBPGs came to the fore here. SBPG 1:20, 1:10:0.4, and 1:10:0.5 could not be tested as a dielectric layer due to insufficient stiffness. We observed that these gels failed to maintain their structural integrity and disintegrated under applied pressure. Therefore, the control group is limited to the SBPGs with stiffness greater than 10 kPa. Plots showing changes in capacitance with respect to applied pressure are provided in **Figure 2**a and Figure S15 (Supporting Information). According to the measurements, the sensitivity trends of the fabricated sensors follow the trends in ionic conductivity and areal capacitance shown by the SBPGs. The most promising sensitivity values are obtained for the sensors with a dielectric layer containing NaCl. The obtained sensitivity values decrease from 1:10:0.3 to 1:10:0.1 as shown in Table S2 (Supporting Information). These results confirm that the sensing performance of the iontronic pressure sensors is directly related to the intrinsic properties (i.e., ionic conductivity, areal capacitance and stiffness) of the dielectric layer.

In addition to the intrinsic properties, the morphology of the dielectric layer affects the sensing performance of the iontronic pressure sensors. For this purpose, sandpaper is used as a mold to texture the SBPGs. SBPG 1:10:0.3 and 1:10:0.2 could not be textured due to insufficient stiffness and excessive stickiness. SBPG 1:10:0.1 is textured successfully and used as the dielectric layer of the iontronic pressure sensors to determine the effects of dielectric morphology on sensitivity. SEM images and 3-D topography of the patterned SBPG showing its 3D morphology are provided in Figure S16a–c (Supporting Information). As provided in Figure 2b, four distinct linear sensing regions are obtained for t-C-1:10:0.1. The sensitivities these regions are 0.124, 565 514,

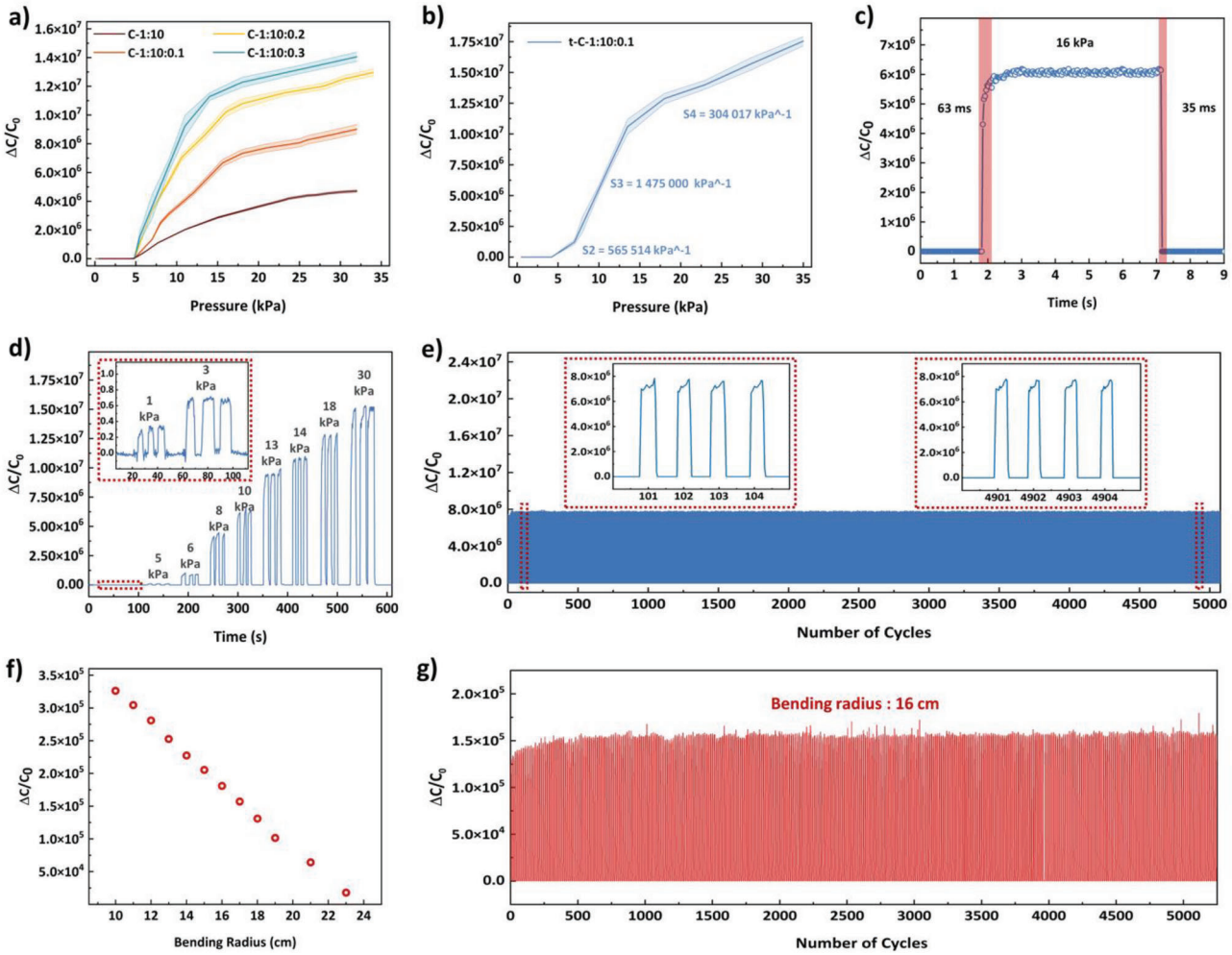

Figure 2. Characterization of the fabricated iontronic pressure sensors. a) Relative capacitance changes of the C-1:10, C-1:10:0.1, C-1:10:0.2, and C-1:10:0.3 with respect to applied pressure (Error bands demonstrate the standard deviation of the measurements). b) Relative capacitance changes of the t-C-1:10:0.1 with respect to applied pressure. Calculated sensitivity values are provided in the figure (Error bands demonstrate the standard deviation of the measurements). c) Response and recovery times of the t-C-1:10:0.1 under a pressure of 16 kPa. d) Relative capacitance changes for t-C-1:10:0.1 under various pressures. e) Capacitance change for the t-C-1:10:0.1 under 12 kPa of cyclic compression. f) Relative capacitance change for t-C-1:10:0.1 as a function of bending radius. g) Response of the sensor over 5000 bending cycles with a bending radius of 16 cm.

1 475 000, and 304 017 kPa^{-1}, between 0 and 4, 4 and 8, 8 and 14, and 18 and 35 kPa, respectively. t-C-1:10:0.1 gives the highest sensitivity among the fabricated iontronic pressure sensors (Table S2, Supporting Information) (Figure S17, Supporting Information shows Region 1 in detail and Figure S18, Supporting Information shows the sensitivity of the textured and untextured sensors). The significant increase in sensitivity can be attributed to the enhancement in surface area upon texturing.[28] Therefore, further characterization of the iontronic pressure sensor is conducted on t-C-1:10:0.1.

Response and recovery times of the sensor under a pressure of 16 kPa are provided in Figure 2c and calculated as 63 and 35 ms, respectively. Repeatable capacitive response of the sensor is demonstrated under various cyclic loadings ranging from 1 to 30 kPa (Figure 2d). Fabricated sensors are capable of detecting very small pressure changes. This is demonstrated by placing bird feathers on the sensors (Figure S19a,b, Supporting Information). The sensor can successfully resolve pressures as small as 1 and 2 Pa as well as the medium pressures including 50 and 100 Pa. These results demonstrated that the fabricated sensor can successfully detect a wide range of pressure changes. The mechanical stability of the sensor is tested through 5000 compression cycles at 12 kPa (Figure 2e). As can be seen, highly stable and proportional responses are recorded from the fabricated sensors, thanks to the remarkable stiffness of the SBPG. The inset Figure show the sensor's response to the first and last four cycles out of a total of 5000 cycles. Almost identical responses prove the robustness of the sensor under cyclic compression. The response of the sensor under bending is also investigated. The capacitance of the sensor increases with decreasing bending radius (Figure 2f). This change is related to the increasing applied compressive pressure on the textured dielectric structure with decreasing bending

Table 1. Recently published iontronic pressure sensors with their active materials, electrochemical characteristics, and sensor characteristics.

Ref.	Electrode material	Dielectric material	Conductivity of the dielectric layer	Areal capacitance	Sensor test frequency	Maximum sensitivity
[13]	$Ti_3C_2T_x$ MXene	PVA/KOH gel	–	–	–	46 730 kPa^{-1}
[28]	Au	PVA/H_3PO_4 gel	–	–	1 kHz	3302.9 kPa^{-1}
[29]	Au	PVA– [Li]+[TFSI]– $Ti_3C_2T_x$ MXene	–	≈30 nF (@1 Hz)	1 kHz	5.5 kPa^{-1}
[30]	Ag NW	P(VdF-HFP)/[EMIM][TFSI] solid polymer electrolyte	–	2.34 μF cm^{-2} (@ 20 Hz)	–	131.5 kPa^{-1}
[17]	Au	Fabric– ([BMIM].PF_6)	–	–	10 kHz	13.5 kPa^{-1}
[31]	Ag Nw	PVDF-[BMIM].PF_6	–	–	100 kHz	1.194 kPa^{-1}
[32]	Graphene	([EMIM]+[BF4]–) droplet	–	–	–	31.1 kPa^{-1}
This work	Carbon black-cellulose-glycerol composite	HEC-glycerol-NaCl supramolecular bio-polymer gel	9.85×10^{-4} S cm^{-1}	12 μF cm^{-2} (@100 Hz)	1 kHz	1 4750 000 kPa^{-1}

PVA: Poly(vinyl alcohol), KOH: Potassium hydroxide, H_3PO_4: Phosphoric acid, [Li]+[TFSI]–: bis(trifluoromethane)sulfonimide lithium salt P(VdF-HFP): Poly(vinylidene fluoride-co-hexafluoropropylene), ([EMIM]+[BF4]–): 1-ethyl-3-methylimidazoliu mtetrafluoroborate [EMIM][TFSI]: 1-ethyl-3-methylimidazolium bi(trifluoromethylsulfonyl)-imide, Ag NW: Silver nanowire, PU: Polyurethane, [EMIM][OTF]: 1-ethyl-3-methylimidazolium trifluoro methanesulfonate, ([BMIM].PF_6): 1-butyl-3-methylimidalium-hexafluorophosphate, PVDF: Poly(vinylidene fluoride), PEGDA: Poly(ethylene glycol) diacrylate, HOMPP: 2-hydroxy-2-methylpropiophenone.

radius. Moreover, stability of the sensor under bending cycles is also tested. After more than 5000 bending cycles, the sensor shows no change in the measured signal amplitude, as can be observed in Figure 2g. Moreover, performance of the fabricated iontronic pressure sensor was evaluated at different relative humidity values, results of which are provided in Figure S20. Under two different humidity conditions, t-C-1:10:0.1 showed very stable pressure response.

We have also compared our best iontronic pressure sensor and its components with recently published articles in the literature (**Table 1**). It is clear that our sensor significantly outperforms its counterparts in terms of sensitivity. Design features play an important role in obtaining significant sensor characteristics. Detailed electrochemical characterization of active layers allow a deep understanding of the iontronic sensing performance.

2.3. Pressure Sensing Mechanism

We employed 3D Bode and 3D areal capacitance analyses to make interpretations about sensing mechanism and the spatial relation between active layers (electrode and dielectric layers) in four linear sensing regions (**Figure 3**a,b, Supporting Information). Detailed explanations about the Bode analysis can be found in the Text S6 (Supporting Information).

In Region I (up to 4 kPa), the spacer forms an air gap between the upper electrode and the dielectric layer, resulting in the creation of an electrode blocking layer. This blocking layer prevents the formation of EDL, resulting in a drastically low initial capacitance. Effects of the electrode blocking layer can be observed in the 3D Bode analysis (Figure 3c). The graph shows that the phase angle of the sensor is almost equal to −90° up to 4 kPa, implying ideal capacitive behavior and contribution of the EDL is not observed. The 3D areal capacitance analysis also confirmed this behavior. Within the test frequency, the capacitance of the sensor is measured in pF levels. In this region, the sensor works with the classical capacitive sensing principles. The capacitance change only depends on the decrease in the distance between the electrode layers and the increase in the effective dielectric constant of the system due to air leaving the structure.[9] The low-pressure sensitivity is attributed to the classical capacitive behavior in this region.

Region II (between 4 and 8 kPa) is the transition region where sensing mechanism evolves from classical capacitive to iontronic sensing. The upper electrode and the ionically conductive dielectric layers start to touch each other. This means that the electrode blocking layer disappears and EDL forms between the layers. The frequency dependent behavior of the areal capacitance proves the formation of EDL (Figure 3d). At the beginning of Region II, the value of the phase angle is measured as −5.43° at 1 kHz, meaning that the leading mechanism of the system has both resistive and capacitive elements due to the air gaps left between the top electrode and the dielectric layer (Figure 3b). The air gaps are responsible for the capacitive contribution, while the surfaces in contact are responsible for the resistive contribution to the impedance of the system. Electrochemical interpretation of the system was provided as a circuit diagram in Region II of the figure. With increasing pressure, the contact area between the electrode and the dielectric layer increases. The change in the value of the phase angle from −6° to −0.2° confirms this behavior (Figure 3c).

Region III begins right after the complete elimination of the air gaps. In this region, a gapless contact occurs between the top electrode and the dielectric layers. After full contact between two successive layers, the device exhibits a resistive behavior that can be inferred from 3D Bode analyses. The sensor's phase angle remains nearly constant from the beginning of Region III to the end of Region IV. Phase angle is −0.2° and increases with the frequency, as shown in Figure 3c. In Regions III and IV, a gradual increase in pressure causes mechanical deformation of the textured dielectric layer. Therefore, the thickness of the layer decreases and the measured areal capacitance value increases throughout the test frequency range (Figure 3d). The main parameter that

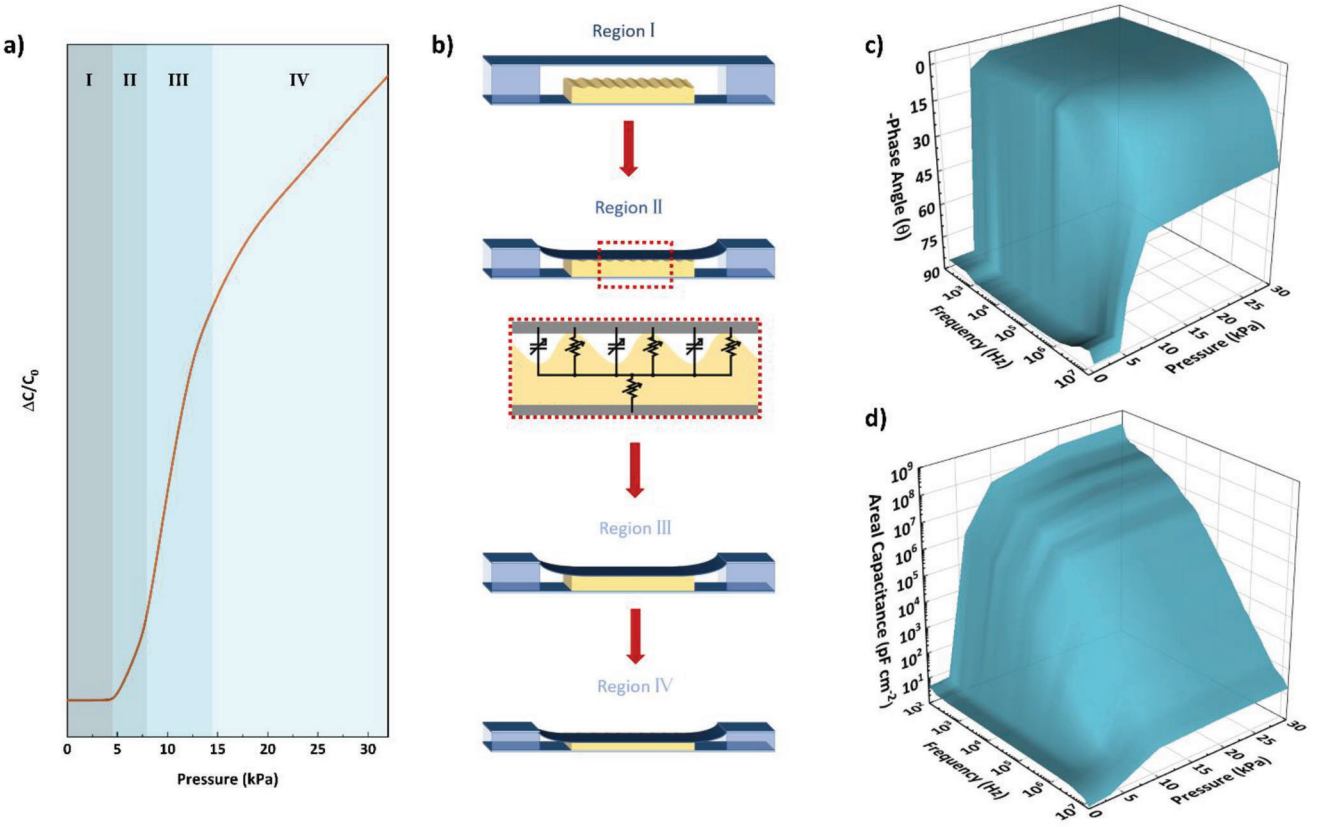

Figure 3. The sensing mechanism of the fabricated iontronic pressure sensors. a) A schematic showing the relative capacitance changes with applied pressure on the sensor. b) Illustrations of the sensor and the spatial relation between active layers in Region I, II, III, and IV. c) 3D Bode graph in negative phase angle, frequency, and applied pressure on the sensor. d) 3D areal capacitance graph with respect to frequency and the applied pressure on the sensor.

determines the capacitance change in these regions is the degree of thickness change due to pressure. Finally, equivalent circuit of the iontronic pressure sensor is provided in Figure S21 (Supporting Information) based on the conducted analyses.

2.4. Smart Glove for Object Recognition

We have fabricated smart gloves using our sensors to demonstrate the full potential of the high sensitivity of the sensors. First a smart glove is fabricated using eight sensing units, as shown in **Figure 4**a. Sensor connections are made using conductive fibers. The sensors are placed on the fingertips and three critical points on the palm. The sensors detected the pressures exerted on these specific areas by the objects being held.

An object recognition test is conducted using 11 common objects. Details of the procedure is provided in Methods. Figure 4b-i–v shows the posture of the hand while holding a billiard ball, tennis ball, plastic ball, PingPong ball, and beaker and their pressure distribution over the iontronic pressure sensor (bottom figure), respectively. Holding positions and the pressure distributions of the remaining objects are provided in Figure S22a–f (Supporting Information).

Object recognition applications in literature with tactile gloves focus on the development of a grid of pressure sensors distributed over the hand. The pressure distribution obtained for each object is treated as an image. The images are then fed into deep learning architectures such as Convolutional Neural Nets for classification.[19] In striking contrast, we fabricated a tactile glove using a much smaller grid, including only 8 highly sensitive iontronic pressure sensors. Therefore, given the small number of input sources, we opted for training conventional supervised machine learning models.

The classification results based on models are summarized in Tables S3 and S4 (Supporting Information). We obtained a classification accuracy of around 90% with Random Forest, Decision Tree, SVM and k-NN classifiers. Paired sensor readings for the object are provided as scatter plot matrix in Figure S23 (Supporting Information) with the exception of the pen and bottle objects, the classifiers are able to distinguish all 11 objects with high positive predictive values and low false discovery rates (Figure 4c). The standard deviation observed over the sensors for each correct and incorrect prediction in Figure 4c indicates the contribution of S1 on both bottle and pen predictions of the model. Due to the slender shape of the bottle, it seemed to cause a pen-like pressure distribution, which could contribute to mutual confusion. The high sensitivity of the sensors seemed particularly effective at distinguishing between four different types of balls (e.g., ping–pong, plastic, tennis, and billiard balls) with different weights. Overall, the high accuracy, precision and recall

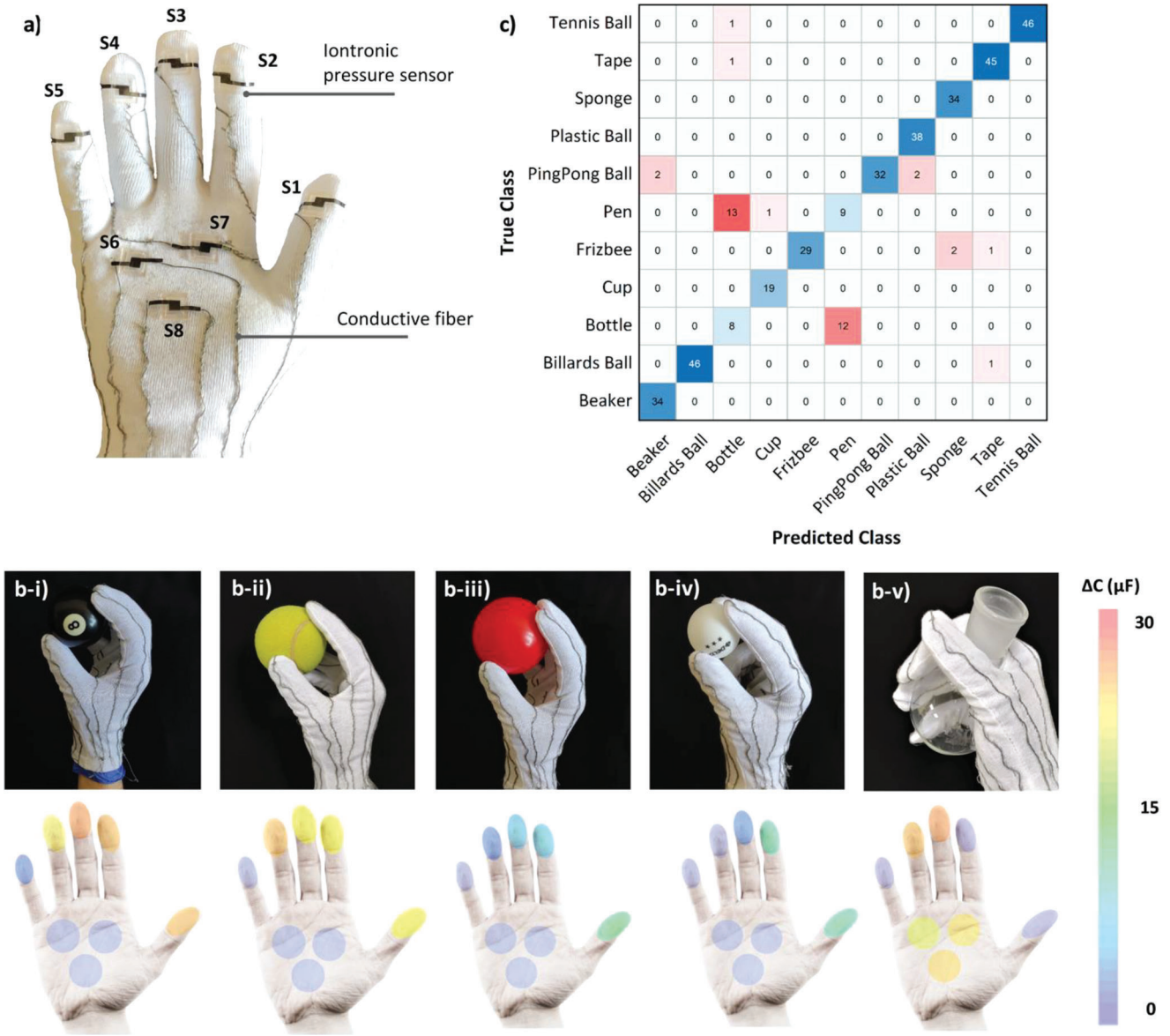

Figure 4. SBPG based iontronic pressure sensor for smart gloves. a) Photograph of a smart glove with eight sensing units that are distributed over the hand. b-i–v) Posture of the hand while holding various objects (including billiard ball, tennis ball, plastic ball, PingPong ball, and beaker) and their pressure distribution over the iontronic pressure sensors. c) The confusion matrix for the Decision Forest classifier. The values inside each cell represent the frequency of occurrence of each case (e.g., the column for bottle shows in the 20 instances the model predicted "bottle" as the outcome, 8 of them actually corresponded to a true bottle case, whereas 12 of them were actually predicted as pen) during the 5–fold validation phase.

measures achieved with as few as eight tactile sensors highlight the potential of this approach to develop tactile sensing applications in human–computer interaction and robotic environments.

This work allowed us to fabricate state-of-the-art iontronic pressure sensors. We have found that dielectric layers with outstanding electrochemical properties and high stiffness are essential to achieve high performance. High performance is translated into high accuracy while using only a limited number of sensors for object recognition from tactile feedback. We rationally designed the SBPG dielectric layers of iontronic pressure sensors using extensive chemical and electrochemical characterization. This design strategy can be extended to other electrochemical devices such as batteries and supercapacitors to achieve unprecedented device performance.

3. Conclusions

In summary, ultra-high sensitivity (1 475 000 kPa^{-1}) iontronic pressure sensors are fabricated using rationally designed SBPG dielectric layers. Extensive characterizations allowed us to determine the ideal HEC: glycerol: NaCl ratio in fabricating SBPGs with an ionic conductivity of 9.85×10^{-4} S cm^{-1}. The working mechanism of the iontronic pressure sensors under dynamic pressures has been interpreted with 3D Bode and areal

capacitance analyzes and the relationships between them are explained in detail. Iontronic pressure sensors are used in a smart glove for object recognition from tactile feedback. The unprecedented sensitivity allowed us to achieve a prediction accuracy of 90% using only eight sensing units.

4. Experimental Section

Materials Characterizations: All characterizations were conducted at 25 °C and 30% relative humidity, unless otherwise specified. Scanning electron microscopy (SEM) (FEI NOVA NANO SEM 430) was used for the morphological characterization of the patterned SBPG layer and the carbon-based electrode layers at an operating voltage of 20 kV. 3D surface topography of the patterned SBPG layer was determined by a Huvitz HRM 300 optical microscope. For XRD analysis of the SBPG layers, a Rigaku Ultima-IV system with Cu Kα radiation (0.154 nm) was used at a scan rate of 2 °C min^{-1}. FTIR analyses were conducted via attenuated total reflection (ATR) unit of the spectrometer (Bruker Alpha Platinum spectrometer) with a resolution of 2 cm^{-1} and 64 scans in the range of 400–4000 cm^{-1}. Thermogravimetric Analysis (TGA) was conducted via Exstar SII TG/DTA 7300 with a temperature increment rate of 10 °C min^{-1}.

Rheological characterization of as-prepared SBPGs was conducted using oscillatory rheometry tests. All tests were performed using a rheometer (Anton Parr, MCR 102) equipped with a parallel plate geometry (diameter of 25 mm) with a gap of 0.4 mm. Frequency sweep tests were conducted to investigate the frequency dependency of storage (G′) and loss modulus (G") under 1% strain at angular frequency values between 0.6 and 3140 rad s^{-1}.

A four-point probe station (Signatone Pro-4) and a Keithley 2400 sourcemeter was used for the surface resistance measurements of the carbon electrodes. Electrochemical tests were conducted using symmetric stainless-steel electrodes within Swagelok cells. HP 4194A Impedance/Gain-Phase Analyzer was used to conduct electrochemical measurements between 100 Hz and 15 MHz. SBPG samples with a thickness and diameter of 400 µm and 8 mm were used for electrochemical characterizations, respectively. Measurements were made with four different samples from different batches for each SBPG composition.

Sensor Characterizations: A LCR Meter (Twintex LCR-7200) was used for the characterization of the sensors. Test frequency was set as 1 kHz for all measurements conducted under 25 °C and 30% relative humidity conditions. Oscillation level of the measurements was also set to 0.1 V. PCE-DFG N digital dynamometer was used to detect the pressure applied to the sensor unless otherwise specified. Measurements were made with four different sensor samples from different batches for each SBPG composition.

Fabrication of the Mold for Texturing: A 188-grit sandpaper was used as the mold. PDMS base and curing agent are mixed (Sylgard 184) in a ratio of 10:1. The prepared solution was poured onto sandpaper and cured at 90 °C for 30 min. Following curing, PDMS was carefully removed from the sandpaper and used as a negative template for patterning the SBPG layer.

Fabrication of the SBPG Layers: HEC (Sigma Aldrich, average molecular weight ≈380 000) was added to DI water and stirred vigorously at 80 °C. A 2.6 mL of DI water was used to dissolve each 0.1 g of HEC. After obtaining a clear solution, the specified amount of NaCl (Merck) was added to the solution (if the layer contains NaCl) and stirred at 80 °C for 30 min. Finally, a certain amount of glycerol was added to the solution and stirred vigorously for 6 h to obtain a homogeneous mixture. Before pouring the solution into the molds, the solution was brought to rest at room temperature for 1 h to eliminate the air bubbles. Following the elimination of bubbles, a specified amount of the solution was poured into the molds and molds are placed into a furnace at 90 °C for 12 h. At the end of the fabrication process, the thicknesses of the SBPG gels were determined as 400 µm.

SBPG solution was poured onto the previously prepared negative PDMS mold to get sandpaper textured SBPG layer for the iontronic pressure sensor. Afterward, it was placed into a furnace at 90 °C for 12 h.

The stoichiometry of SBPGs was controlled by keeping the amount of glycerol constant and varying the amounts of HEC and NaCl. Constituent ratios of the gels were provided in Table S1 (Supporting Information).

Fabrication of Carbon-Based Electrodes: Carbon-cellulose electrodes were prepared via simple solution mixing and doctor blading methods. 1 g of HEC was added to 20 mL of DI water and dissolved under magnetic stirring at 80 °C. Once a clear solution was obtained, carbon black (CB, Alfa Aesar, 50% compressed) was (0.5, 1, or 1.5 g) added slowly to ensure proper mixing and stirred overnight to obtain a homogeneous suspension. Then, 1 g of glycerol was added to the suspension and further stirred at 80 °C for at least 2 h to obtain an ink-like suspension. Prior to casting, the prepared suspension was ultrasonicated for 1 h to increase homogeneity. Afterward, prepared ink-like suspension was cast onto glass substrates using the doctor blade method at a wet thickness of 300 µm. Glass substrates were previously washed with acetone, ethanol, and DI water and treated with a high-frequency spark generator to obtain a hydrophilic surface. Casted films were dried under ambient conditions overnight and peeled off to obtain flexible, self-standing carbon-cellulose films as the electrodes. Finally, fabricated carbon electrode sheets were cut into the desired shapes using a marking laser (FiberLAST-NanoMark Energy Series (10 W, 1064 nm wavelength, 100 ns pulse length, 100 mm s^{-1}spee

Fabrication of the Iontronic Pressure Sensor: The fabricated sensors were composed of four main elements: substrates, carbon-based electrodes, SBPG iontronic layer, and spacers. PET substrates with a thickness of 70 µm and an area of 1.25 × 1.25 cm^2 were used as the substrate for the sensor. The carbon-based electrodes with an area of 0.5 × 0.5 cm^2 were glued onto the PET substrates using PDMS. A PDMS-curing agent mixture (1:10 ratio) was prepared, well-mixed, and brush painted onto the PET substrate. After curing the PDMS layer in an oven at 90 °C for 30 min, electrode layers, PDMS, and the PET substrate were found to adhere firmly to each other. Prepared SBPG layer was placed to the bottom electrode. 1.5 mm thick VHB tape, serving as a spacer, was placed on the edges of the PET substrates. This spacer also insulates the sensor and protects the SBPG layer from environmental factors such as moisture that can affect the gel's structure.

Fabrication of the Smart Gloves: Previously fabricated, eight sensors (t-C-1:10:0.1) were placed onto specific locations of the knitted glove. Conductive threads were used for the electrical connections of the sensors.

Object Recognition: During each trial, the experimenter grasped each object for a duration of ≈30 s while the pressure readings were obtained at 1.33 Hz. The trials were cut at the onset and the end of each grasp, which produced a recording with average duration of 25.6 s (SD = 7.19) per object. The final dataset included a total of 376 labeled readings obtained from 8 sensors distributed over the hand.

The machine learning models including Naïve Bayes, Support Vector Machines (SVM), k-Nearest Neighbors (kNN), Random Forest, Discriminant Analysis, and Decision Tree classifiers were trained by using the MATLAB R2020a Classification Learner toolkit. The data were randomly split into 60%, 20%, and 20% chunks for training, testing and validation, respectively. 100 iterations were carried out during hyperparameter optimization with fivefold cross-validation.

Ethical Statement: Written consent is obtained from the users who have used the gloves for experiments. The ethics committee approval is obtained from METU Human Research Ethics Committee (312-ODTU-2021).

Supporting Information

Supporting Information is available from the Wiley Online Library or from the author.

Acknowledgements

Ismail Eken is greatly acknowledged for his support on illustrations. The authors also would like to thank Irmak Karakaya for the valuable discussions on the FTIR analysis.

Conflict of Interest

The authors declare no conflict of interest.

Data Availability Statement

The data that support the findings of this study are available from the corresponding author upon reasonable request.

Keywords

flexible electronics, human–machine interfaces, iontronic pressure sensors, machine learning, object sensing

Received: February 28, 2023
Revised: June 7, 2023
Published online: June 26, 2023

[1] Y. Yang, T. Cui, D. Li, S. Ji, Z. Chen, W. Shao, H. Liu, T. L. Ren, *Nano-Micro Lett.* **2022**, *14*, 161.
[2] M. Shi, H. Wu, J. Zhang, M. Han, B. Meng, H. Zhang, *Nano Energy* **2017**, *32*, 479.
[3] M. Kaltenbrunner, T. Sekitani, J. Reeder, T. Yokota, K. Kuribara, T. Tokuhara, M. Drack, R. Schwödiauer, I. Graz, S. Bauer-Gogonea, S. Bauer, T. Someya, *Nature* **2013**, *499*, 458.
[4] T. Li, H. Luo, L. Qin, X. Wang, Z. Xiong, H. Ding, Y. Gu, Z. Liu, T. Zhang, *Small* **2016**, *12*, 5042.
[5] J. Huang, M. Zhao, Y. Cai, M. Zimniewska, D. Li, Q. Wei, *Adv. Electron. Mater.* **2020**, *6*, 1900934.
[6] M. A. U. Khalid, M. Ali, A. M. Soomro, S. W. Kim, H. B. Kim, B. G. Lee, K. H. Choi, *Sensors Actuators, A Phys.* **2019**, *294*, 140.
[7] Y. Lu, G. Yang, Y. Shen, H. Yang, K. Xu, *Nano-Micro Lett.* **2022**, *14*, 150.
[8] D. Doganay, M. O. Cicek, M. B. Durukan, B. Altuntas, E. Agbahca, S. Coskun, H. E. Unalan, *Nano Energy* **2021**, *89*, 106412.
[9] M. O. Cicek, D. Doganay, M. B. Durukan, M. C. Gorur, H. E. Unalan, *Adv. Mater. Technol.* **2021**, *6*, 2001168.
[10] S. Abolpour Moshizi, S. Azadi, A. Belford, A. Razmjou, S. Wu, Z. J. Han, M. Asadnia, *Nano-Micro Lett.* **2020**, *12*, 109.
[11] R. Li, Y. Si, Z. Zhu, Y. Guo, Y. Zhang, N. Pan, G. Sun, T. Pan, *Adv. Mater.* **2017**, *29*, 1700253.
[12] Y. Chang, L. Wang, R. Li, Z. Zhang, Q. Wang, J. Yang, C. F. Guo, T. Pan, *Adv. Mater.* **2021**, *33*, 2003464.
[13] L. Gao, M. Wang, W. Wang, H. Xu, Y. Wang, H. Zhao, K. Cao, D. Xu, L. Li, *Nano-Micro Lett.* **2021**, *13*, 140.
[14] M. B. Durukan, M. O. Cicek, D. Doganay, M. C. Gorur, S. Çınar, H. E. Unalan, *Adv. Funct. Mater.* **2021**, *32*, 2106066.
[15] Z. Shen, X. Zhu, C. Majidi, G. Gu, *Adv. Mater.* **2021**, *33*, 2102069.
[16] Y. Ren, Z. Liu, G. Jin, M. Yang, Y. Shao, W. Li, Y. Wu, L. Liu, F. Yan, *Adv. Mater.* **2021**, *33*, 2008486.
[17] Q. Lin, J. Huang, J. Yang, Y. Huang, Y. Zhang, Y. Wang, J. Zhang, Y. Wang, L. Yuan, M. Cai, X. Hou, W. Zhang, Y. Zhou, S. G. Chen, C. F. Guo, *Adv. Healthcare Mater.* **2020**, *9*, 2001023.
[18] Y. Luo, Y. Li, P. Sharma, W. Shou, K. Wu, M. Foshey, B. Li, T. Palacios, A. Torralba, W. Matusik, *Nat. Electron.* **2021**, *4*, 193.
[19] S. Sundaram, P. Kellnhofer, Y. Li, J. Y. Zhu, A. Torralba, W. Matusik, *Nature* **2019**, *569*, 698.
[20] Z. Zhu, R. Li, T. Pan, *Adv. Mater.* **2018**, *30*, 1705122.
[21] H. Liu, Y. Yu, F. Sun, J. Gu, *IEEE Trans. Autom. Sci. Eng.* **2017**, *14*, 996.
[22] M. Köhler, P. Lunkenheimer, A. Loidl, *Eur. Phys. J. E: Soft Matter* **2008**, *27*, 115.
[23] C. A. C. Sequeira, A. Hooper, *Solid State Ionics* **1983**, *9–10*, 1131.
[24] Z. Li, S. Zhang, Y. Chen, H. Ling, L. Zhao, G. Luo, X. Wang, M. C. Hartel, H. Liu, Y. Xue, R. Haghniaz, K. J. Lee, W. Sun, H. J. Kim, J. Lee, Y. Zhao, Y. Zhao, S. Emaminejad, S. Ahadian, N. Ashammakhi, M. R. Dokmeci, Z. Jiang, A. Khademhosseini, *Adv. Funct. Mater.* **2020**, *30*, 2003601.
[25] M. Capurro, F. Barberis, *Evaluating the Mechanical Properties of Biomaterials*, Woodhead Publishing Limited, Netherlands **2014**.
[26] G. Meng, W. H. Ko, *Sens. Actuators, A* **1999**, *75*, 45.
[27] W. H. Ko, Q. Wang, *Sens. Actuators, A* **1999**, *75*, 242.
[28] N. Bai, L. Wang, Q. Wang, J. Deng, Y. Wang, P. Lu, J. Huang, G. Li, Y. Zhang, J. Yang, K. Xie, X. Zhao, C. F. Guo, *Nat. Commun.* **2020**, *11*, 209.
[29] S. Sharma, A. Chhetry, S. Zhang, H. Yoon, C. Park, H. Kim, M. Sharifuzzaman, X. Hui, J. Y. Park, *ACS Nano* **2021**, *15*, 4380.
[30] A. Chhetry, J. Kim, H. Yoon, J. Y. Park, *ACS Appl. Mater. Interfaces* **2019**, *11*, 3438.
[31] Q. Liu, Z. Liu, C. Li, K. Xie, P. Zhu, B. Shao, J. Zhang, J. Yang, J. Zhang, Q. Wang, C. F. Guo, *Adv. Sci.* **2020**, *7*, 2000348.
[32] J. S. Kim, S. C. Lee, J. Hwang, E. Lee, K. Cho, S. J. Kim, D. H. Kim, W. H. Lee, *Adv. Funct. Mater.* **2020**, *30*, 1908993.